Russian Chemical Reviews **70** (8) 627 – 639 (2001) © 2001 Russian Academy of Sciences and Turpion Ltd

DOI 10.1070/RC2001v070n08ABEH000678

Scanning tunnelling vibrational spectroscopy of single surface complexes and detection of single electron spins

F I Dalidchik, S A Kovalevskii, B R Shub

Contents

I.	Introduction	627
II.	Single molecule chemical physics of surfaces	628
III.	Threshold and resonance features of currents flowing through nanoscale tunnel junctions containing adsorbed species	628
IV.	Inelastic electron tunnelling spectroscopy with STM	630
V.	Vibrational scanning tunnelling spectroscopy using resonance features of STM currents	631
VI.	Kinetics of vibrational and spin transitions in single surface complexes	634
VII.	Scanning tunnelling spectroscopy using fluctuations of STM currents	637
VIII.	Time-resolved scanning tunnelling spectroscopy	637
IX.	Conclusion	637

Abstract. New spectroscopic techniques employing the scanning tunnelling microscope are considered. The new methods allow measurements of the vibrational spectra of single surface complexes, determination of the nonequilibrium distributions of such complexes over vibrational levels, studies on the kinetics of vibrational transitions, determination of vibrational relaxation parameters, detection of single surface electron spins and studies on the dynamics of fast surface migration of species. The physical grounds and possible applications of the methods in chemical research are also discussed. The bibliography includes 80 references.

I. Introduction

Determination of the structure and properties of surface complexes belongs to the key problems of modern chemical physics of surfaces including heterogeneous catalysis. The number of differently organised groups of adsorbed species can be rather large even in the simplest systems. For instance, the interaction of oxygen with metals can be accompanied by the formation of more than ten types of complexes, depending on the metal crystal face involved in the process, the metal oxidation state and temperature. These complexes differ not only in their adsorption sites, but also in atomic and electronic structure. Usually, such complexes coexist and interact with one another at sufficiently high coverages of the surface. In heterogeneous catalysis, the most reactive complexes play the role of active surface sites.[1, 2]

Different surface complexes can play the role of active surface sites in different stages of a catalytic reaction, *i.e.*, in the course of adsorption and surface migration and in various chemical transformations (dissociation, desorption, as well as substitution, recombination or exchange reactions). The internal structure and properties of the surface complexes have long been intensively studied by many experimental methods. However, the exact nature of the active surface sites remains a moot question as yet for the majority of systems including those studied in most detail. Determination of the exact nature faces great difficulties which are mainly associated with a large number of types of surface complexes and with low steady-state concentrations of the active sites due to their high reactivity.

Experiments with structurally and chemically homogeneous surfaces (the so-called 'ideal' surfaces) are free from these drawbacks. Carrying out high-vacuum experiments allows one to assemble macroscopic ensembles of regularly arranged surface complexes of a particular type by controlled low-temperature adsorption on microfacets of perfect single crystals.[3] The structure and properties of such systems can be studied in detail by various spectroscopic methods including optical and corpuscular ones, beam and field emission techniques, as well as steady-state and kinetic methods.[4] It should be noted that most of the widely used methods have initially been developed to study the dynamics of elementary processes in the gas phase.

Experiments with ideal surfaces have significantly extended the ideas of both the internal structure of surface structures and the dynamics of elementary acts in heterogeneous processes. In such experiments, many complexes have been found for the first time. Beam experiments provided direct evidence for the dependence of the reactivity of ideal surfaces on their atomic structure.[5] Femtosecond laser experiments allowed the characteristic times of electronic and vibrational relaxation of many surface complexes to be measured for the first time.[6] Currently, heterogeneous processes on ideal surfaces are studied with a time resolution of $\sim 10^{-13} - 10^{-14}$ s, which is sufficient for the real-time observation of the motion of individual species (molecules, ions, atoms) in elementary acts of chemical transformations.

Since 1960s, intensive studies of ideal surfaces as model systems have been carried out in many countries. The results of such studies serve as one of the main sources of information necessary for devising physical models of the interactions of atomic species with the surface and at the solid surfaces. However, the results of high-vacuum measurements bear no direct relation to the chemistry of real surfaces. Typically, the time taken to form a real surface is of the order of 10^{-7} s ($P \approx 1$ atm, $T \approx 300$ K). Such surfaces are characterised by disordered atomic structures. In real systems, the variety of types of ensembles of surface

F I Dalidchik, S A Kovalevskii, B R Shub N N Semenov Institute of Chemical Physics, Russian Academy of Sciences, ul. Kosygina 4, 119991 Moscow, Russian Federation. Fax (7-095) 137 83 18.
Tel. (7-095) 939 72 59 (F I Dalidchik), (7-095) 939 73 52 (S A Kovalevskii), (7-095) 137 82 73 (B R Shub)

Received 27 April 2001
Uspekhi Khimii **70** (8) 715 – 729 (2001); translated by A M Raevsky

complexes is much greater than in ideal systems. Often, real surfaces are covered by complexes that cannot be produced in desired amounts in high-vacuum experiments to be studied then by conventional spectroscopic methods such as IR, Auger and ESR spectroscopy, *etc*. Additionally, the dynamics of elementary acts of various heterogeneous processes in ordered and disordered ensembles of the same surface complexes can be essentially different. For chemisorbed species this is due to changes in the potential energy surfaces upon the formation of new chemical bonds, whereas in the case of physisorbed particles the distinctions can be due to multiple scattering of both products and reagents by the species surrounding the reacting complex.

Compared to modelling of gas-phase processes, the problem of devising physical models of heterogeneous surface reactions is much more complicated. The dynamics of all essential elementary gas-phase processes can be studied in detail using high-vacuum beam and optical experiments. However, the results of such experiments with ideal surfaces are insufficient to devise physical models of heterogeneous chemical reactions, especially catalytic ones, which are of prime interest in practice. Studies on the dynamics of elementary acts of gas-phase reactions can be successfully performed with femtosecond time resolution, which allows real-time monitoring of the motion of atomic species. In the case of heterogeneous chemical reactions, solving a similar problem requires not only real-time, but also real-space monitoring of the motion of atomic species and, hence, atomic-scale spatial resolution. The present state-of-the-art in chemical physics of surfaces is characterised by great demand for novel methods which would allow assembling of single complexes of adsorbed species at specified points of the surface, studies on their atomic and electronic structure, measurements of physical parameters, determination of chemical properties and studies on the dynamics of elementary acts of chemical transformations at the single-event level. Currently, the development of such methods requires the use of scanning tunnelling microscopy (STM). Hence, the new methods should be basically different from those used in studies of gas-phase processes.[7,8]

II. Single molecule chemical physics of surfaces

In experiments with STM, the atomic and electronic structure of conducting surfaces is probed with a thin metallic tip (the radius of curvature of well-fabricated tips is comparable with the characteristic atomic size) separated from the surface by a distance d of the order of 5–10 Å.[8] In this case, the overlap of the atomic orbitals of the tip and the surface is very weak and the surface–tip system represents a nanoscale tunnel junction whose conductance

$$\sigma = \frac{\partial J}{\partial V},$$

(J is the current and V is the voltage) at low voltages ($V \ll \varphi$, φ is the tip work function) is determined by the probability of electron tunnelling through the potential barrier (the barrier penetrability)

$$D(d) \propto \exp\left(-2d\sqrt{2\varphi}\right) \qquad (1)$$

and by the surface local density of electron states [$\rho(\varepsilon,\mathbf{r})$] at the position of the tip[9]

$$\sigma(V) \propto D(d)\rho[\varepsilon(V),\mathbf{R}], \qquad (2)$$
$$\varepsilon(V) = \varepsilon_F - V.$$

Here, ε and $\mathbf{r}$ are the energy and coordinate of an electron, respectively, $\mathbf{R}$ is the tip coordinate and ε_F is the Fermi level. (In the text below, we will use the system of atomic units, except otherwise specified; the tip polarity is assumed to be negative.)

According to relationship (2), displacements of the tip across the surface (at specified V and d) produce changes in the current flowing through the tunnel junction, which are proportional to the changes in the electron density $\rho[\varepsilon(V),\mathbf{R}]$, which are determined by the relief of the surface. For 'single-atom' tips, where the tunnelling current is determined by the overlap of the surface orbital with the orbital of the atom nearest to the surface, one gets $\delta J/\delta R \approx 0.1$ nA Å^{-1}. This is sufficient for 'current' imaging of a surface area with Ångström spatial resolution by simply scanning it. Spectroscopic measurements, *i.e*., measurements of the $\sigma - V$ dependences allow reconstruction of the energy distributions of electrons at specified points of the surface. [Note that relationships (1) and (2) include only the contribution of elastic tunnelling characterised by conservation of the energies of the tunnelling electrons. Usually, this is the most probable case.]

The invention of the STM[7] opened a new, amazing world of single-molecule phenomena. The STM is capable of imaging surfaces with Ångström spatial resolution and provides the possibility of seeing individual adsorbed atoms, molecules and adsorbate clusters in the real space, as well as of directly monitoring reconstruction† of ideal surfaces,[10,11] elementary acts of slow surface migration,[12] dissociation[13] and desorption.[14,15] Numerous examples of manipulating individual adsorbed species with the STM tip by their targeted desorption, adsorption, dissociation and transfer between the surface and the tip have been reported. In modern experiments with STM, the atomic and electronic structure of surfaces covered by adsorbed species are studied at the single complex level while the dynamics of heterogeneous processes is in increasing frequency studied at the single-event level. Chemical physics of surface becomes a 'single molecule' science.[16]

The opportunities of 'single molecule' chemical physics of surface seem to be almost boundless, especially taking into account continuous evolution of spectroscopic methods which make it possible to obtain information on the structure of single surface complexes and the dynamics of individual acts of elementary chemical transformations. Experiments with STM allow one not only to see individual adsorbed species and complexes and to reconstruct the corresponding electron energy distributions, but also to measure their vibrational spectra,[17,18] create and measure different types of nonequilibrium vibrational distributions[19] and reconstruct parameters of heterogeneous vibrational[20,21] and electronic[22,23] relaxation. It is also possible to study the kinetics of spontaneous and current-induced vibrational transitions in single surface complexes. (It is this kinetics that often determines the probabilities of elementary acts of chemical transformations of the complexes located under the tip of an STM.[21]) Recently, methods for detection of single surface paramagnetic centres have been proposed and evaluated.[24] Some new experimental schemes have been considered, which would initiate studies on the kinetics of spin transitions in single paramagnetic centres, measurements of spin–lattice relaxation times and relaxation times of individual electronically excited physisorbed molecules[22,23] and research in the field of detection of single molecule magnetic resonance effects.[25–27] New methods for STM studies on the dynamics of fast migration of those adsorbed atomic species whose stable images cannot be obtained have been proposed and theoretically substantiated.[28,29] The main goal of this review is to describe and analyse recent advances in single molecule heterogeneous chemistry.

III. Threshold and resonance features of currents flowing through nanoscale tunnel junctions containing adsorbed species

Most of new spectroscopic methods exploiting STMs also employ the effects of spin-dependent and inelastic electron tunnelling. The former effect is associated with the dependence of tunnelling probability on the electron spin orientation while the latter is due

† Before the invention of the STM, reconstruction of ideal surfaces was studied only by diffraction methods which allow one to obtain raw experimental information about the surface structure in the reciprocal lattice space rather than conventional coordinate space.

to processes in which energy exchange occurs between the tunnelling electrons and electronic and vibrational degrees of freedom of the adsorbed species. In experiments with STM, inelastic electron tunnelling including spin-dependent electron tunnelling can manifest themselves as two kinds of characteristic features on the $J-V$ curves, *viz*., threshold [17] and resonance features.[18]

Threshold features are observed at voltages corresponding to the opening of inelastic electron tunnelling channels. (Below the threshold voltage inelastic tunnelling of an electron is impossible since in this case the electron energy after excitation of a species located under the tip of an STM should be lower than that of the Fermi level corresponding to the highest occupied electron state.) An energy level diagram illustrating both elastic and inelastic electron tunnelling is presented in Fig. 1.

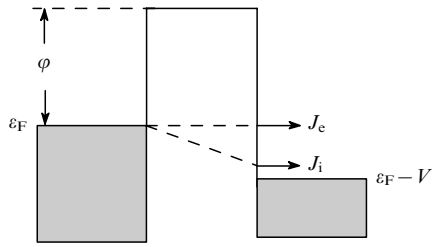


Figure 1. An energy level diagram illustrating electron tunnelling through a nanoscale tunnel junction at voltages $V \ll \varphi$; J_e and J_i are the elastic and inelastic electron tunnelling currents, respectively.

At threshold voltages $V_\omega = \omega$ (ω is the excitation energy of a species located under the STM tip) the conductance of a tunnel junction changes jumpwise

$$\sigma(V) \propto \eta(V - V_\omega), \tag{3}$$

where $\eta(x)$ is the Heaviside function

$$\eta(x) = \begin{cases} 0, & x \leqslant 0 \\ 1, & x > 0 \end{cases}$$

Experiments with STM are usually carried out at $\omega \gg kT$ (k is the Boltzmann constant and T is the temperature of the surface).

The conductance jump magnitude, $\delta\sigma(V_\omega)$, is proportional to the excitation probability of a surface complex, w_ω

$$\delta\sigma(V_\omega) \propto w_\omega \sigma^-(V_\omega), \tag{4}$$
$$\delta\sigma(V_\omega) = \sigma^+(V_\omega) - \sigma^-(V_\omega),$$
$$\sigma^\pm(x) = \sigma(x \pm 0).$$

Resonance features of the STM currents manifest themselves at voltages corresponding to 'bloomed' tunnel junctions (Fig. 2). The effect of resonance blooming of double potential barriers separated by a well with appropriate quasi-stationary electron energy level ε_0 is well known in quantum mechanics.[30] Resonance tunnelling of species involves three stages. A species tunnelling from the left half-space is captured by the well, spends some time in the quasi-stationary state and then tunnels through the second potential barrier to appear in the right half-space. Clearly, the tunnelling probability, $D(\varepsilon)$, is determined by three terms, *viz*., the resonance capture probability, Γ_1, the decay probability of the quasi-stationary state with retention of the initial tunnelling direction, Γ_2/Γ ($\Gamma = \Gamma_1 + \Gamma_2$, where Γ_2 is the probability of tunnelling through the second potential barrier) and the density of electronic states, $\rho_0(\varepsilon)$, near the quasi-stationary energy level ε_0.

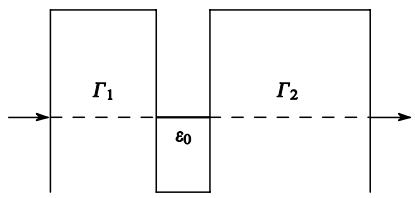


Figure 2. A scheme of tunnelling through the double potential barrier (resonance tunnelling mechanism).

$$D(\varepsilon) \approx \frac{\Gamma_1\Gamma_2}{\Gamma}\rho_0(\varepsilon), \tag{5}$$
$$\rho_0(\varepsilon) = \frac{1}{\pi}\frac{\Gamma}{(\varepsilon - \varepsilon_0)^2 + \Gamma^2}.$$

At $\varepsilon = \varepsilon_0$, the probability of tunnelling through the double potential barrier is equal to the ratio rather than product of the exponentially low probabilities of tunnelling through the single potential barriers

$$D(\varepsilon_0) \approx \frac{\Gamma_{\min}}{\Gamma_{\max}}, \tag{6}$$

where $\Gamma_{\min} = \min(\Gamma_1, \Gamma_2)$, $\Gamma_{\max} = \max(\Gamma_1, \Gamma_2)$. If $\Gamma_1 = \Gamma_2$, one gets $D(\varepsilon_0) = 1$, which means that the 'as-wide-and-high-as-it-wished' double potential barrier appears to be absolutely penetrable. This also holds for those potential barriers which contain electron traps with vibrational degrees of freedom. It has been shown that 'instantaneous' formation and decay of the quasi-stationary electron state can strongly 'shake' the slow vibrational subsystem ($\varepsilon_0 \gg \omega$, ω is the vibrational quantum), thus exciting not only single-quantum, but also multi-quantum vibrational transitions.[31]

The probability of inelastic resonance electron tunnelling, $D_{\upsilon\upsilon'}(\varepsilon)$ (υ and υ' are the vibrational quantum numbers before and after tunnelling), has the form

$$D_{\upsilon\upsilon'}(\varepsilon) = \frac{4\Gamma_1(\upsilon,\bar{\upsilon})\Gamma_2(\bar{\upsilon},\upsilon')}{[\varepsilon - \varepsilon_0(\bar{\upsilon}) + \omega\upsilon]^2 + \Gamma^2}, \tag{7}$$
$$\Gamma_{1(2)}(\upsilon,\bar{\upsilon}) = \Gamma_{1(2)}\langle\upsilon|\bar{\upsilon}\rangle^2,$$
$$\Gamma = \Gamma_1 + \Gamma_2. \tag{8}$$

Here, Γ_1 is the probability of resonance electron capture by the well in the quasi-stationary state (the probability of tunnelling through the first potential barrier), $\varepsilon_0(\bar{\upsilon}) = \varepsilon_0 + \bar{\omega}(\bar{\upsilon} + 1/2)$ is the energy of the vibronic level of the quasi-stationary state, $\bar{\upsilon}$ is the vibrational quantum number of the quasi-stationary state, $\langle\upsilon\bar{\upsilon}\rangle$ are the Franck–Condon factors and Γ_2 is the decay probability of the quasi-stationary state, followed by escape of the electron with retention of the initial tunnelling direction.

It is easily seen that if the potential barriers are characterised by equal Γ_1 and Γ_2 values and the electron energy ε takes its resonance value $\varepsilon = \varepsilon_0(\upsilon,\bar{\upsilon})$, the expression for inelastic tunnelling probability, $D_{\upsilon\upsilon'}(\varepsilon)$, does not contain exponentially small terms and, hence, double potential barriers can also be absolutely penetrable

$$D_{\upsilon\upsilon'}[\varepsilon = \varepsilon_0(\upsilon,\bar{\upsilon})] \propto \langle\upsilon|\bar{\upsilon}\rangle^2\langle\bar{\upsilon}|\upsilon'\rangle^2, \tag{9}$$
$$\varepsilon_0(\upsilon,\bar{\upsilon}) = \varepsilon_0 + \bar{\omega}\left(\bar{\upsilon} + \frac{1}{2}\right) - \omega\left(\upsilon + \frac{1}{2}\right),$$
$$\Gamma_1 = \Gamma_2.$$

It should be noted here that, strictly speaking, simple formula (7) for calculating the probabilities of elastic ($\upsilon = \upsilon'$) and inelastic ($\upsilon \neq \upsilon'$) resonance tunnelling is valid only for long-lived intermediate states ($\Gamma < \bar{\omega}$). On the other hand, the expression for the total tunnelling probability

$$D_\upsilon = \sum_{\upsilon'} D_{\upsilon\upsilon'}, \tag{10}$$

which determines the experimentally measured tunnelling current, is not subject to this limitation [see Ref. 31 which concerns the development of a general theory of inelastic resonance tunnelling and derivation of formulae that are valid at arbitrary ratios between the oscillation period, the lifetime of the quasi-stationary electron state and the times of electron tunnelling through single potential barriers $\tau_{1,2} = (\partial \ln \Gamma_{1,2}/\partial\varepsilon)^{-1}$].

Inelastic resonance tunnelling is a purely quantum-mechanical effect which can be observed in any nanoscale junctions including those formed by the tip of an STM and the surface. In this case, the role of electron traps can be played by adatoms having appropriate energy levels. However, this is a rare case which is of secondary importance. For the species which are of prime interest for practice, such as adsorbed O_2, H_2O, CO molecules, *etc*., the resonance electron energy levels lie below ε_F. The simplest (artificial) way of creating a near-surface electron trap consists of applying a voltage exceeding the tip work function for electrons to the junction.[32,33] Figure 3 presents an energy level diagram illustrating the mechanism of electron tunnelling from the tip to a sample at such voltages, when the STM operates in the field emission mode.[34,35] It is easily seen that in this case the tunnelling path has a segment of classically allowed motion of length l

$$l \approx \frac{V-\varphi}{V} d \approx 5-7\ \text{Å}.$$

At particular energies $\varepsilon_n(V,d)$, standing electron waves (field emission resonances, n is the resonance number) originate in this segment. In other words, a nanoscale resonator is formed near the surface, in which the tunnelling electrons are trapped to spend times

$$t_n \approx \Gamma_n^{-1} \approx \left(\frac{\partial \varepsilon_n}{\partial n}\right)^{-1} (1-\beta)^{-1}. \qquad (11)$$

Here, β is the surface reflection coefficient of an electron with energy ε_n. For pure metals, $\beta \approx 0.1-0.3$ [34,35] and Γ_n values are sufficiently large ($\hbar\Gamma_n \approx 1$ eV, $t_n \approx 4\times10^{-15}$ s), so that the resonance maxima corresponding to different vibrational levels are overlapped. In this case, vibrational transitions of adsorbed species can manifest themselves as small-scale oscillations on the wings of broad field emission resonances.[33] For oxides and metal surfaces coated with thin oxide films, Γ_n values are much smaller [$\hbar\Gamma_n \approx 0.1$ eV, $t_n \approx 4\times10^{-14}$ s (see Refs 18, 19, 24)] and the resonance maxima corresponding to different vibrational transitions can be well resolved. Longer residence times of electrons near such surfaces can be due to the formation of space charge under the tip of the STM injecting electrons into the oxide (the current density $j \approx 10^6-10^8$ A cm^{-2}.)

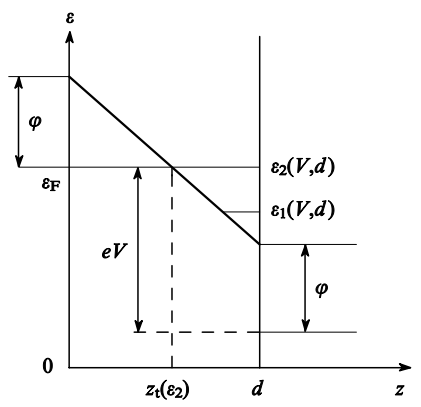


Figure 3. A scheme illustrating electron tunnelling in an STM operating in the field emission mode ($V > \varphi$);
$\varepsilon_{1(2)}(V,d)$ are the electron energy levels of field emission resonances, d is the surface – tip separation and z_t is the classical turning point.

Depending on the atomic and electronic structure of the tip, resonance features on the current – voltage characteristics of the STM can manifest themselves either as conductivity maxima [if $\rho_t(\varepsilon) \approx$ const, where $\rho_t(\varepsilon)$ is the local density of electron states at the position of the tip] or total current maxima [if $\rho_t(\varepsilon)$ exhibits a narrow peak, which is characteristic of 'single-atom' tips and tips containing adsorbed species[36,37]]. In experimental studies of molecular adsorption on the metal and oxide surfaces by vibrational scanning tunnelling spectroscopy using resonance features of STM currents such maxima have been observed in the $J-V$ curves.[18–21,24,38–43]

IV. Inelastic electron tunnelling spectroscopy with STM

1. Single-quantum vibrational transitions of single adsorbed molecules

Threshold features of tunnelling currents in metal – dielectric – metal (M – D – M) junctions containing adsorbed species were predicted and experimentally found in 1966.[44] Threshold features of currents in tunnel $n-p$-junctions (tunnel diodes[45]) due to phonon excitation have been observed by Holonyak and Lesk.[46]

Since energy exchange between an electron and slow vibrational degrees of freedom of the surface is adiabatically forbidden, the probabilities of inelastic tunnelling are usually very low. According to recent estimates,[33] the probabilities of vibrational transitions can be described by a relationship

$$w_{\upsilon,\upsilon'} \propto \left(\frac{a_0}{R_0}\right)^{2|\upsilon-\upsilon'|}, \qquad (12)$$

where a_0 is the zero-point vibrational amplitude and R_0 is the equilibrium position of the oscillator simulating the vibrational subsystem. For single-quantum transitions ($|\upsilon-\upsilon'| = 1$), $w_\omega \approx 0.01-0.05$. Threshold features on the $J-V$ curves of M – D – M tunnel junctions are virtually unobservable. To distinguish them against the background noise, the dependences of $\partial\sigma/\partial V$ on V are usually measured. In this case, threshold features manifest themselves as peaks, the positions of which allow determination of the vibrational quantum energy ω.

Inelastic electron tunnelling spectroscopy of M – D – M tunnel junctions was widely used in 1970 – 1980s for measuring vibrational spectra of species adsorbed at the metal – dielectric interface (see publications on tunnelling vibrational spectroscopy, *e.g*., review[47]). These measurements were performed with macroscopic ensembles of adsorbed species. As a consequence, all the spectra measured by tunnelling vibrational spectroscopy were inhomogeneously broadened. Spectroscopy of threshold features of the STM currents is free from this drawback.

The possibility of observation of threshold features associated with single-quantum vibrational transitions in adsorbed species in experiments with STM seems to be apparent since the energy level diagrams used for illustration of elastic and inelastic tunnelling through M – D – M junctions and nanoscale tunnel junctions are the same (see Fig. 1). In essence, the problem of observation of small-scale threshold features in the experiments with STM is reduced to the problem of capabilities of the instrument the experimentalist has in hand.

As should be expected, single-quantum transition probabilities obtained in theoretical studies of the extent of threshold features of STM currents were estimated at $\sim 0.01-0.05$.[48,49] Search for threshold features due to single-quantum vibrational transitions was carried out in many research laboratories over more than a decade. These studies were stimulated, in particular, by the necessity of solving one of the central problems of STM physics, *viz*., the problem of chemical identification of single adsorbed species, whose topographic images are strongly dependent on the scanning mode (*i.e*., on the specified V and d values).

The first example of a threshold feature associated with single-quantum excitations of stretching vibrations of the C – H bond has been reported only recently by Ho *et al*.[17] who studied

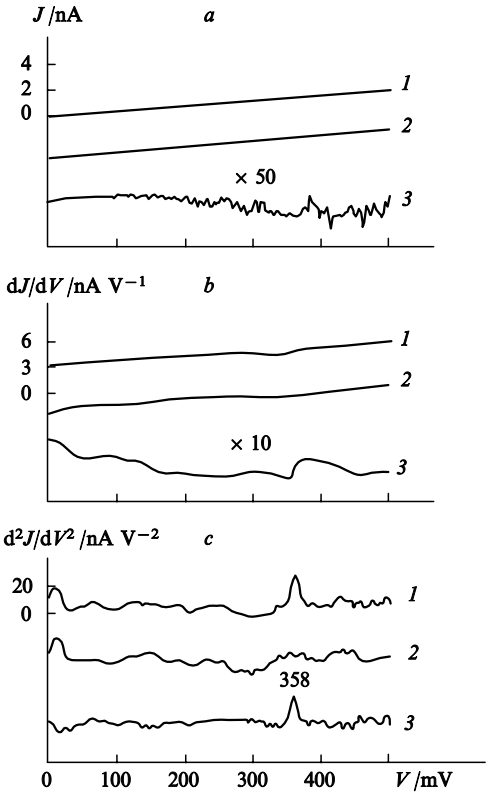


Figure 4. Threshold features of the STM current J (*a*), $\partial J/\partial V$ (*b*) and $\partial^2 I/\partial V^2$(*c*) recorded for a single acetylene molecule adsorbed on the Cu(100) surface.[17]
The curves were recorded with the STM tip positioned over the center of acetylene molecule (*1*) and over the clean surface area (*2*). Curves *3* represent the corresponding difference curves (*1*–*2*). Curves *2* and *3* are shifted along the ordinate axis.

adsorption of a single C_2H_2 molecule on the Cu(100) surface. The design of the new low-temperature STM specially developed to extend the capabilities of inelastic electron tunnelling spectroscopy to a single molecule level has been described elsewhere.[50] Some of the results obtained by Ho *et al.*[17] and presented in Fig. 4 can serve as an illustration of the difficulties associated with extraction of weak threshold signals from the intense background noise of the total current. (Recently,[51] it has been reported that Ho's continuous measurements of the spectra required signal accumulation during many hours.[17]) The isotope effect observed for deutero-substituted acetylene molecules has proven correctness of the assignment of the threshold feature shown in Fig. 4 to single-quantum vibrational transitions of the C–H bond. Later, inelastic electron tunnelling spectroscopy was used to observe elementary acts of dehydrogenation of single ethylene, benzene and pyridine molecules.[52] The topographic images obtained at different time instances allowed observation of displacements and rotations of single molecules, which would be induced by the STM current. Detection of a threshold feature due to the single-quantum vibrational excitations of CO molecules adsorbed on the Cu(001) and Cu(110) surfaces was reported.[53] However, multi-quantum (or combination) vibrational transitions, the probabilities of which do not exceed 0.001 [see expression (12)], have not been observed so far using inelastic electron tunnelling spectroscopy.

2. Electronic transitions in single adsorbed molecules

Conductance jumps of tunnelling gaps, due to vibrational transitions in adsorbed molecules represent an important but not the only example of manifestation of inelastic tunnelling in the experiments with STM. Other interesting examples are associated with electronic excitation of surface complexes. Since in this case there is no small characteristic parameter (energy exchange between two electrons having comparable energies occurs effectively), one should expect that the extent of the threshold features of STM currents associated with electronic transitions in the adsorbed species will be much greater than that observed in the case of vibrational transitions. This problem has been studied recently[22,23] taking a threshold feature associated with the $X^3\sum_g^- - a^1\Delta_g$-transition in physisorbed oxygen molecules as an example. In this case, the threshold feature should be observed at $V \approx 1$ V. Rather high probability of the excitation of oxygen molecules to the singlet state by the tunnelling electrons (the probabilities of such transitions in the gas phase can reach 10% to 15%, see Ref. 54) allows one to predict a new effect, namely, the dependence of the magnitude of the threshold jump on the tunnelling current. At currents $J \approx (w_{TS}\,\tau_{ST})^{-1}$, where w_{TS} is the excitation probability of oxygen molecules from the triplet to the singlet state by inelastically tunnelling electrons and τ_{ST} is the singlet–triplet relaxation time of oxygen, the time intervals between individual electronic transitions between the tip and the surface are insufficient for complete relaxation of the singlet oxygen molecule. Hence, the tunnelling current measured over a time interval $t \gg \tau_{ST}$ ($t \approx 10^{-3}$ s, $\tau_{ST} \approx 10^{-8}$ s) consists of two components,

$$J = J_T n_T + J_S n_S, \qquad (13)$$
$$J_{T(S)} = J_{eT(S)} + J_{iT(S)}.$$

The currents $J_{T(S)}$ are due to the tunnelling electrons which interact with the molecule that was initially in the triplet (singlet) state. In both cases, elastic and inelastic electron tunnelling is possible [the corresponding currents are $J_{eT(S)}$ and $J_{iT(S)}$]. The latter process, which is responsible for the formation of singlet oxygen, has a threshold

$$J_{iT} \propto \eta(eV - \hbar\omega_S),$$

where $\hbar\omega_S$ is the excitation energy of singlet oxygen ($\hbar\omega_S \approx 1$ eV).[1] The probabilities of different events (different types of tunnelling) are proportional to the time-average populations of the triplet and singlet states (n_T and n_S, respectively), which are determined by the kinetics of spontaneous (relaxation) and current-induced transitions. By varying the STM current (this can be done by simply changing the distance between the surface and the STM tip), *i.e.*, by changing the ratio of the excitation and relaxation rates one can achieve targeted variation of the parameters $J_{T(S)}\tau_{ST}$, which will affect the populations and, hence, the magnitude of the threshold feature of the STM current. The minimum tunnelling currents (J_{min}) at which the dependence of the conductance jump on J is observed will determine the singlet–triplet relaxation time of a single singlet oxygen molecule ($\tau_{ST} \approx J_{min}^{-1}$).

V. Vibrational scanning tunnelling spectroscopy using resonance features of STM currents

1. Multi-quantum and combination vibrational transitions in single molecules adsorbed on the oxide and metal surfaces

Measurements of vibrational spectra of surface complexes are widely used in studies of chemical processes on the surfaces of solids. Absorption IR spectroscopy,[55] electron energy loss spectroscopy,[56] tunnelling vibrational spectroscopy[47] and other versions of vibrational spectroscopy allow identification of main types of surface complexes and determination of their structure. However, these methods provide only averaged information about macroscopic ensembles of species (see above) and single-quantum vibrational transitions in them. Recently,[18–20,38,40] the method of vibrational scanning tunnelling spectroscopy (VSTS) has been developed. This technique, which uses an STM operating in the field emission mode, allowed the vibrational spectra of adsorbed species to be measured for the first time in experiments

with STM. As a rule, the bands observed in such spectra correspond to not only single-quantum, but also multi-quantum vibrational transitions including combination ones. These spectra allow virtually unambiguous chemical identification of the species located under the STM tip.

Vibrational series of field emission resonances, which allowed the first observation of the effects of inelastic resonance electron tunnelling in experiments with STM, were predicted and detected in 1997.[18] The first experiments with a commercial STM Omicron (Germany) were carried out on naturally oxidised titanium samples in air. The current–voltage characteristics obtained exhibited clearly defined groups of equidistant maxima. The current *vs.* voltage ($J-V$) dependences were measured at different points of the surface at constant separation d of the order of 5 Å, which was adjusted and maintained by choosing an appropriate current at $V_{max} = 10$ V. The currents J varied from 4 to 20 nA. The $J-V$ dependences were measured with variable V increments ranging from 0.01 to 0.05 V. To exclude small-scale fluctuations of the measured currents, the results obtained with the 0.01 V increment were averaged over two (four) close V values. It was found that at weak currents $J(V_{max})$ resonance lines appear on the $J-V$ curves only at $V > 8$ V. At $J(V_{max}) > 7$ nA, resonance features were clearly seen in the whole range of changes in V, that is, from 5 to 10 V ($\varphi \approx 5$ eV). An example of the vibrational spectra measured in the study cited [18] is shown in Fig. 5. Comparison of the measured vibrational quanta (0.1 eV) with those known for TiO_2 ($\hbar\omega \approx 0.09$ eV) allowed one to assign these lines to the vibrational transitions of the Ti–O bond. Simultaneously, spectra with $\hbar\omega \approx 0.27$ and 0.45 eV were also observed.[18] These quanta were associated with vibrational transitions in the adsorbed CO molecules and OH radicals. Further experiments were carried out in ultrahigh vacuum ($P < 10^{-9}$ Torr) with dosed adsorption of the gases under study.

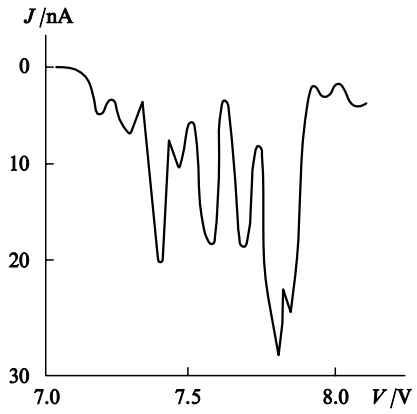


Figure 5. Vibrational spectrum of oxidised titanium ($\hbar\omega = 0.1$ eV).[18]

2. Adsorption of water on oxidised titanium. Isotope effect

Oxides are widely used as supports for many types of catalysts.[1,2] Adsorption of water on oxide surfaces has been repeatedly studied by different methods (see, *e.g.*, Ref. 57); nevertheless, one of the key issues, *viz.*, that of the forms of adsorption, remained open until the performance of the VSTS experiments.

The first measurements of the vibrational spectra of water adsorbed on the titanium surface oxidised in air using high-vacuum experiments with STM have been reported recently.[40] (This 'in-air' method was also used for measuring the vibrational spectra of water adsorbed in the nanoscale junction formed by the Ir–Pt tip and niobium.[58]) Measurements of the $J-V$ curves were preceded by a special procedure for the preparation of the surfaces under study, which included heating of samples to 550 K followed by long-term storage in high vacuum and exposure of the samples

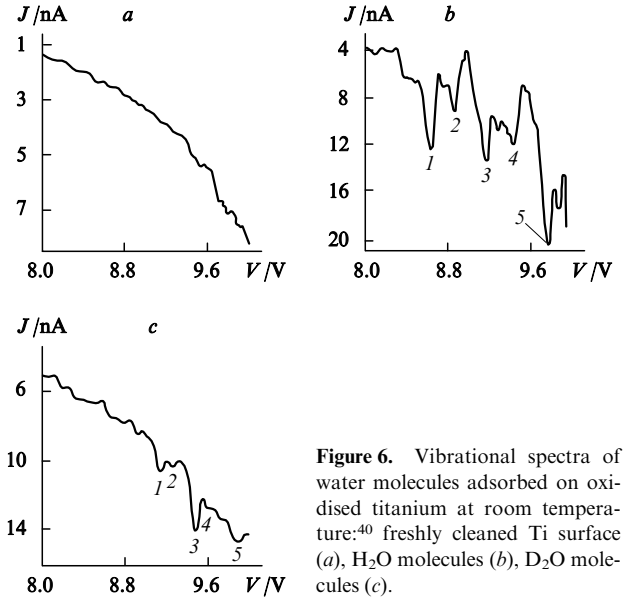


Figure 6. Vibrational spectra of water molecules adsorbed on oxidised titanium at room temperature:[40] freshly cleaned Ti surface (*a*), H_2O molecules (*b*), D_2O molecules (*c*).

to water vapour at a pressure of $\sim 10^{-6}$ Torr. After heating of the samples for ~ 2 h and subsequent storage in high vacuum the current–voltage characteristics measured at the majority of the surface points exhibited faintly visible series of field emission resonances corresponding to the vibrational frequencies of titanium oxide (see Fig. 6 *a*). Further exposure of the sample to water vapour (~ 300 K) was accompanied by significant changes in the spectral pattern; in particular, measurements at many surface points gave the spectra similar to that shown in Fig. 6 *b*. This spectrum exhibits clearly defined resonance lines corresponding to the single-quantum [$\hbar\omega_1 \approx e(V_3 - V_1) \approx 0.5$ eV, $\hbar\omega_2 \approx e(V_2 - V_1) \approx 0.2$ eV], two-quantum [$\hbar\omega_3 \approx e(V_5 - V_1) \approx 2\hbar\omega_1$] and combination [$\hbar\omega_4 \approx e(V_4 - V_1) \approx \hbar\omega_1 + \hbar\omega_2$] vibrational transitions in water molecule (the subscript at the quantities ω and V denotes the number of the resonance line in the spectrum). Small-scale maxima between the first and second (and between the third and fourth) resonances in Fig. 6 *b* correspond to the vibrations of the Ti–O bond ($\hbar\omega \approx 0.1$ eV). The magnitudes of the quanta $\hbar\omega_1$ and $\hbar\omega_2$ were found to be close to the known IR spectroscopy data on the stretching [$\hbar\omega_1(\mathrm{IR}) = 0.46$ eV] and bending [$\hbar\omega_2(\mathrm{IR}) = 0.20$ eV] vibrational quanta of H_2O molecules adsorbed on the oxidised titanium surface. It was found that the surface areas characterised by the spectra similar to that shown in Fig. 6 *b* have an island structure with the island size from 10 to 50 nm (this is typical of water adsorption on the surface of polycrystals). Blank runs with heavy water (D_2O) also gave similar spectra (see Fig. 6 *c*) with field emission resonances with the energies $\hbar\omega_1(D_2O) \approx 0.35$ eV and $\hbar\omega_2(D_2O) \approx 0.15$ eV. With an accuracy of $\sim 10\%$, this corresponded to the expected isotope effect

$$\frac{\hbar\omega(H_2O)}{\hbar\omega(D_2O)} \approx \sqrt{2}.$$

The shift of vibrational spectra towards smaller $\hbar\omega$ values represents the main, but not the only manifestation of the isotope effect. Replacement of hydrogen by deuterium leads to simultaneous change in frequency and the vibronic coupling parameter α

$$\frac{\alpha_D}{\alpha_H} \approx \sqrt{2}.$$

Correspondingly, the Franck–Condon factors determining the extent of the resonance maxima also change. For instance, for the transitions ($0 \rightarrow 1$) one gets

$$\frac{\langle 0|1\rangle_{\rm H}}{\langle 0|1\rangle_{\rm D}} = \frac{\alpha_{\rm H}}{\alpha_{\rm D}} \exp[-(\alpha_{\rm H} - \alpha_{\rm D})].$$

These relationships allow estimation of the parameter $\alpha_{\rm H}$. Using experimental data

$$\frac{J^{\rm r}_{\rm H}(\upsilon = 1)}{J^{\rm r}_{\rm D}(\upsilon = 1)} \approx 1.25,$$

where $J^{\rm r}_{\rm H,D}$ are the resonance components of the current (*i.e.*, the heights of the resonance maxima, calculated relative to the background curve), we get $\alpha_{\rm H} \approx 1.4$.

The observation of the isotope effect in the spectra of resonance features on the $J-V$ curves of the STM is unambiguous evidence for correspondence between the observed series of resonance maxima (see Fig. 6 *b*,*c*, peaks *1*–*5*) and vibrational transitions in the adsorbed water molecules. The absence of lines at $\hbar\omega \approx 0.2$ eV in particular spectra (see, *e.g.*, Fig. 7) suggests that the surface complex represents an OH radical (the value $\hbar\omega \approx 0.5$ eV corresponds to the stretching vibrational quantum of the OH radical). Hence, both types of adsorption (*viz.*, molecular and dissociative ones) on the TiO_2 surface are possible at room temperature, as was suggested recently.[57]

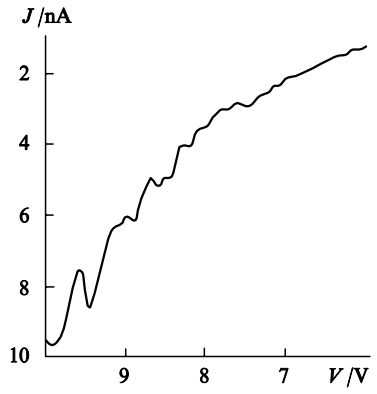


Figure 7. Vibrational spectrum of hydroxyl group adsorbed on oxidised titanium at room temperature.[41]

Vibrational scanning tunnelling spectroscopy (or spectroscopy of resonance features of STM currents) opens considerable opportunities for studies on the adsorption of various gases on the surface of oxides and metals coated with thin oxide films. The method allows one for the first time to obtain reliable chemical identification of the adsorbed species and to measure the spectra of not only single-quantum, but also multi-quantum vibrational transitions including combination ones in the adsorbed molecules and clusters. This has been exemplified by oxygen clusters adsorbed on the Al(100) surface at room temperature.[20, 39, 42]

3. Multi-quantum vibrational transitions in oxygen clusters adsorbed on aluminium

Initial stages of aluminium oxidation have been intensively studied by many experimental methods including scanning tunnelling microscopy,[59] high-resolution electron energy loss spectroscopy,[60, 61] IR spectroscopy, *etc*. Currently, it is known that at room temperature and low surface coverages the adsorbed oxygen forms small clusters with characteristic vibrational quanta $\hbar\omega_1 = 0.11-0.12$, $\hbar\omega_2 = 0.07-0.08$ and $\hbar\omega_3 = 0.036-0.040$ eV.[59–61] Low-energy electron diffraction studies[60, 61] showed that the intensities of the electron energy loss peaks depend on the oxygen dose to which the sample was exposed. At small doses [$< 10-20$ Langmuir (L), 1 L = 1 Torr s], the losses were found to be ~ 0.08 and 0.12 eV. Exposure to greater doses ($\gtrsim 100$ L) corresponding to the formation of nanoscale islands on

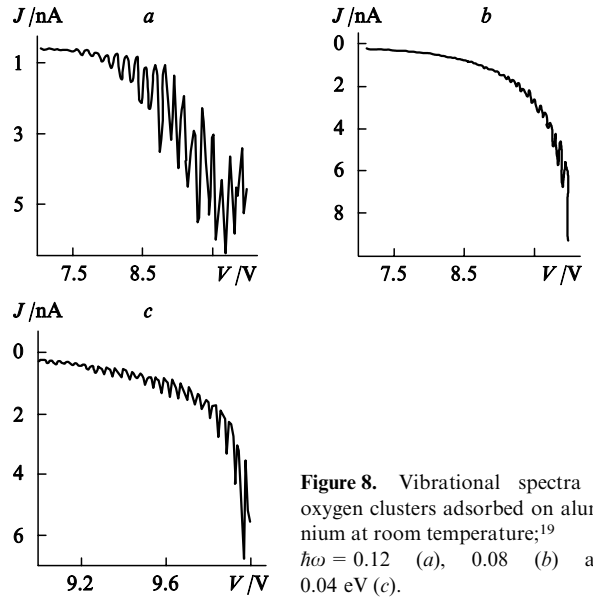


Figure 8. Vibrational spectra of oxygen clusters adsorbed on aluminium at room temperature;[19] $\hbar\omega = 0.12$ (*a*), 0.08 (*b*) and 0.04 eV (*c*).

the surface of the oxide phase resulted in the losses $\hbar\omega = 0.04$ eV. The same $\hbar\omega$ values were obtained [19] in the VSTS measurements of vibrational spectra of oxygen adsorbed on the Al(100) surface (Figs 8–10).

Experiments with the Al(100) and oxidised titanium surfaces were carried out using the same procedures for both the preparation of the surfaces and measurements of vibrational spectra with the STM. The $J-V$ curves measured for clean Al(100) surface with an increment $\Delta V = 0.01$ V exhibited no resonance features and were well described by the Fowler–Nordheim formula

$$J(V) = \exp\left(-\frac{C}{V}\right) \qquad (14)$$

($C = 10-100$ V), which corresponds to electron tunnelling from the tip of an STM operating in the field emission mode.

Measurements at different points of the surface carried out at $\sim 10-20$ L doses showed that nearly 10% of the $J-V$ curves exhibited vibrational series with $\hbar\omega_1 \approx 0.12$ eV. (The spectra with $\hbar\omega_2 \approx 0.08$ eV were observed more rarely.) This allows the determination of the sticking coefficient of oxygen to the clean Al(100) surface, $\theta \approx 0.005-0.01$. The same values were obtained in a STM study of the initial stages of Al(100) oxidation.[59]

Exposure to greater doses was accompanied by significant changes in the pattern of vibrational spectra. For instance, spectra with $\hbar\omega_3 = 0.04$ eV appeared at different points of the surface at

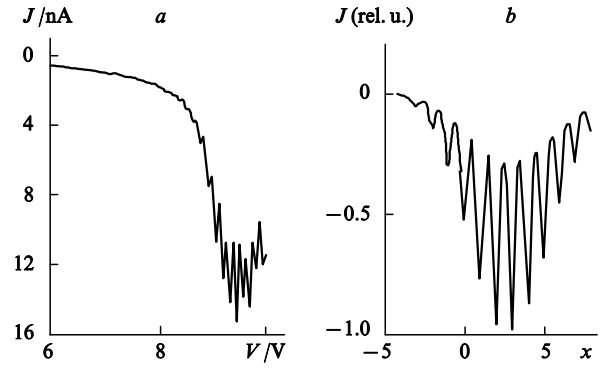


Figure 9. Vibrational spectrum of oxygen cluster adsorbed on aluminium ($\hbar\omega = 0.12$ eV, dose 20 L);[19] bell-shaped envelope (*a*) and theoretical curve calculated using formula (6) for the Boltzmann distribution over vibrational levels, $x = V/\omega$ (*b*).

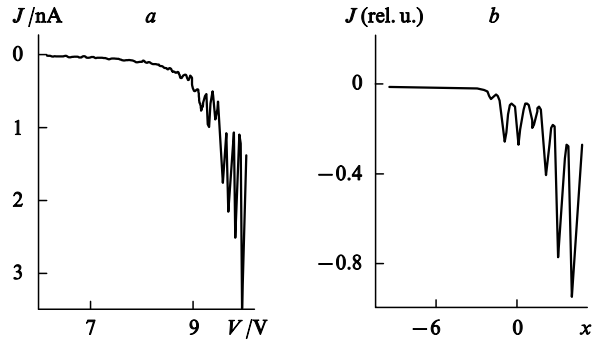


Figure 10. Vibrational spectrum of oxygen cluster adsorbed on an aluminium surface ($\hbar\omega = 0.12$ eV, dose 20 L);[19]
oscillating envelope (*a*) and theoretical curve calculated using formula (6) for the inverse distribution over vibrational levels (*b*).

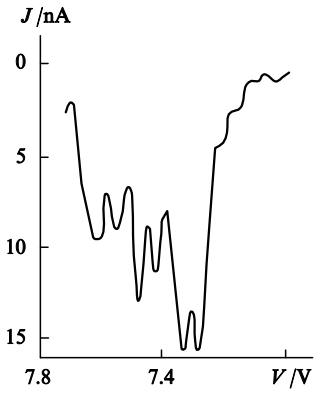


Figure 11. Doubled vibrational series of field emission resonances for paramagnetic radical ion O_2^- adsorbed on oxidised titanium (the effect of exchange splitting of resonance lines).[24]

50 L doses. Further increase in exposure doses led to a decrease in the number of spectra with the lines with larger $\hbar\omega$ (0.12 and 0.08 eV) and to rapid increase in the number of spectra with the vibrational quantum $\hbar\omega_3 = 0.04$ eV corresponding to the oxide phase. After exposure to $\sim$1000 L doses the $J-V$ curves measured at almost all points of the surface under study exhibited long series of resonance maxima corresponding to the oxide. Simultaneously, adsorption of CO molecules on the oxidised aluminium surface was observed. Such complexes can be readily identified using their spectra that exhibit lines corresponding to combination vibrational transitions

$$eV_{\upsilon_1\upsilon_2} = eV_0 + \hbar\omega_0\upsilon_1 + \hbar\omega_3\upsilon_2, \quad \upsilon_{1,2} = 0, 1, 2, \ldots, \tag{15}$$

where the largest vibrational quantum [$\hbar\omega_0 = 0.24$ eV (see Ref. 61)] equals the well-known value characteristic of the CO molecules.

4. Detection of single surface paramagnetic centres

The surfaces of oxides and oxidised metals are always covered by small amounts of paramagnetic centres [$< 1\%$ (see Ref. 2)] which are usually studied by ESR on polycrystals.[62] Attempts at detecting ESR signals from individual paramagnetic centres (PC) with the STM have been undertaken.[63, 64] Weak changes in the tunnelling currents were detected in experiments with oxidised silicon. Signals were observed at room temperature at distances $\sim$3 to 6 Å from the single point defects tentatively identified as PC. Such a dependence of the ESR signal on the tip position seems to be abnormal. The origination mechanism of 'single-atom' ESR in the case of equally populated Zeeman levels is currently unknown. The problem of integration of the ESR and STM methods needs further consideration.

Possible variants of such an integration have been considered.[25, 26] It was shown that using ferromagnetic tips (here, the tunnelling electrons are polarised) allows detection of ESR signals in the experiments with STM even at room temperature when $kT > \hbar\omega_L$ (ω_L is the Larmor frequency) and the Zeeman levels have equal equilibrium populations. This can be done with the operating currents $J > \tau_\sigma^{-1}$ (τ_σ is the characteristic spin–lattice relaxation time) at which the polarised tunnelling electrons create nonequilibrium distributions over the Zeeman levels. Practical implementation of this technique would make it possible to reveal the arrangement of paramagnetic centres on the surface using the capabilities of the STM; however, these experiments preclude measurements of *g*-factors since local magnetic fields under the ferromagnetic tip of the STM are currently unknown.

Another solution to the problem of detection with STM of a single PC has been suggested and evaluated.[24, 65] It was found that for metal oxides and metals coated with thin oxide films, the exchange splitting of the field emission resonances ($\delta_{j,n}$) can be larger than or comparable with the width of the energy level: $\delta_{j,n} \approx 0.1-0.2$ eV, $\Gamma_{j,n} \leqslant 0.1-0.04$ eV. Hence it follows that the vibrational spectra of the PC should have the form of two series of equidistant maxima on the $J-V$ curves, shifted with respect to each other by the exchange splitting $\delta V \approx 0.1-0.2$ V.

Such a spectrum has first been observed for oxidised titanium (Fig. 11). Based on the exchange splitting and the vibrational quantum magnitude ($\hbar\omega = 0.15$ eV), this PC can be unambiguously identified as a single surface paramagnetic radical ion O_2^-. [The vibrational frequency of dioxygen ion adsorbed on oxide surfaces is well known from the IR spectroscopy data:[2] $\hbar\omega(O_2^-) = 1180\ \text{cm}^{-1} = 0.15$ eV.] The characteristic spectral pattern corresponding to the adsorbed radical ion O_2^- represents a complete spin-vibrational 'portrait' of this species, which can also be used in studies of single O_2^- ions adsorbed on other surfaces. This can be exemplified by the spin-vibrational spectrum of a single O_2^- ion detected on the oxidised Al(100) surface (Fig. 12).

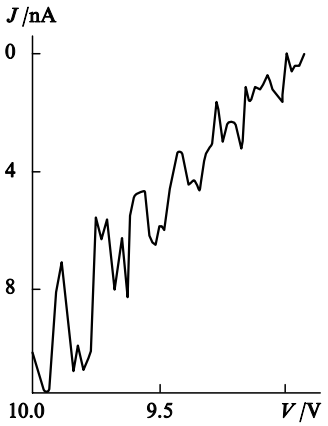


Figure 12. Spin-vibrational series for paramagnetic radical ion O_2^- adsorbed on oxidised aluminium surface.

VI. Kinetics of vibrational and spin transitions in single surface complexes

The development of new methods for detection with STM of single paramagnetic centres and measurements of multi-quantum vibrational spectra of single surface complexes creates prerequisites for the invention of 'kinetic' modifications of the scanning tunnelling spectroscopy of vibrational and spin transitions. This is of crucial importance.

According to the ergodic hypothesis, the kinetics of quantum transitions can be studied by two equivalent approaches. One of

them implies experiments with ensembles of identical subsystems while the other involves experiments with the same subsystem and multiple repetition of the transitions under study. Until recently, all kinetic modifications of spectroscopic methods were based on the first approach. However, spectroscopic measurements with ensembles can appear to be insufficiently informative in the case of inhomogeneous systems such as surfaces covered with adsorbed species. Scanning tunnelling spectroscopy of vibrational and spin transitions allows the second approach to be implemented for the first time. (In this case, the kinetics of quantum transitions in ensembles of elementary events occurring in the same surface complex rather than in ensembles of adsorbed species is studied.) These surface chemistry studies were impossible[‡] until recent publications.[18, 19, 22]

The idea of kinetic scanning tunnelling spectroscopy is very simple. In experiments with STM, the current densities can be as high as 10^{10} to 10^{11} A cm^{-2}. Thus, the time intervals between individual acts of tunnelling can be shorter (or at least comparable with the characteristic relaxation times of internal degrees of freedom of the surface complexes.) At such electron current densities, the distributions of the species located under the STM tip over vibrational states appear to be essentially nonequilibrium. If ferromagnetic tips are used, spin distributions of the species also appear to be nonequilibrium.[25, 26] Under these conditions, the average current J measured during the time of the order of 10^{-3} s includes contributions of a large number of transitions,

$$J(V) = \sum_{\upsilon,S,S_z} n(\upsilon, S, S_z) J_{\upsilon,S,S_z}(V). \tag{16}$$

Here, $n(\upsilon,S,S_z)$ is the current-dependent population of the state $|\upsilon,S,S_z\rangle$ of the surface complex 'sitting' under the STM tip, J_{υ,S,S_z} is the tunnelling current due to the electrons interacting with the species which initially was in the state $|\upsilon,S,S_z\rangle$ and S and S_z are the spin of the species and its projection, respectively.

Since individual acts of electron tunnelling are uncorrelated (the relaxation times of electronic subsystems for the surface and tip are much shorter than all other characteristic times), the kinetics of vibrational and spin transitions in the surface complex can be described by a system of balance equations

$$\frac{\partial n(v)}{\partial t} = \sum_{vv'} \left[n(v') w_{v'v} - n(v) w_{vv'} \right] = 0, \tag{17}$$

where v denotes the totality of vibrational and spin quantum numbers and $w_{v'v}$ are the probabilities of quantum transitions $v' \to v$, which, generally, can be both current induced and spontaneous (relaxation)

$$w_{v'v} = J_{v'v} + w_{\mathrm{r}\, v'v}\,. \tag{18}$$

Here, $J_{v'v}$ are the tunnelling currents corresponding to the electronic transitions for particular fixed initial (v') and final (v) values of the vibrational and spin quantum numbers of the complex and $w_{\mathrm{r}\, v'v}$ are the probabilities of spontaneous transitions.[§] Taken together, the system of equations (17) and expressions (16) and (18) make it possible to obtain a self-consistent description of the formation of resonance features on the $J-V$ curves of the STM. Resonance currents $J_{v'v}$ can be calculated using formula (7). According to expression (16), the series of field emission resonances on the $J-V$ curves depend on the distributions $n(v,S,S_z)$, which allows their reconstruction from experimental data.[19, 20, 25] From Eqns (17) and expression (18) it follows that the dependence of the distributions $n(v,S,S_z)$ on $w_{\mathrm{r}\, v'v}$ can be used for reconstructing the kinetics of spin and vibrational transitions.

Some examples of nonequilibrium spin effects, potentially observable in systems with ferromagnetic tips, have been considered recently.[25] Therefore, below we will restrict ourselves to the description of nonequilibrium effects which can be observed in the vibrational spectra of adsorbates.[19, 20]

1. Reconstruction of nonequilibrium distributions over vibrational states

The relation between the shape of the envelopes of vibrational spectra of adsorbed species and the distributions $n(\upsilon)$ can be easily understood by analysing a diagram of vertical vibrational transitions occurring in the case of capture of a tunnelling electron by a trap (resonator). Such a diagram illustrating the main model of multi-quantum vibrational transitions (the model of shifted harmonic oscillators[67]) is shown in Fig. 13. (Recent estimates[24] have shown that the vibrational frequencies of adatoms change by no more than 10% to 15% upon capture of an electron by the resonator.) It is easily seen that for the equilibrium vibrational distributions corresponding to rather weak tunnelling currents insufficient for strong heating of the vibrational subsystem

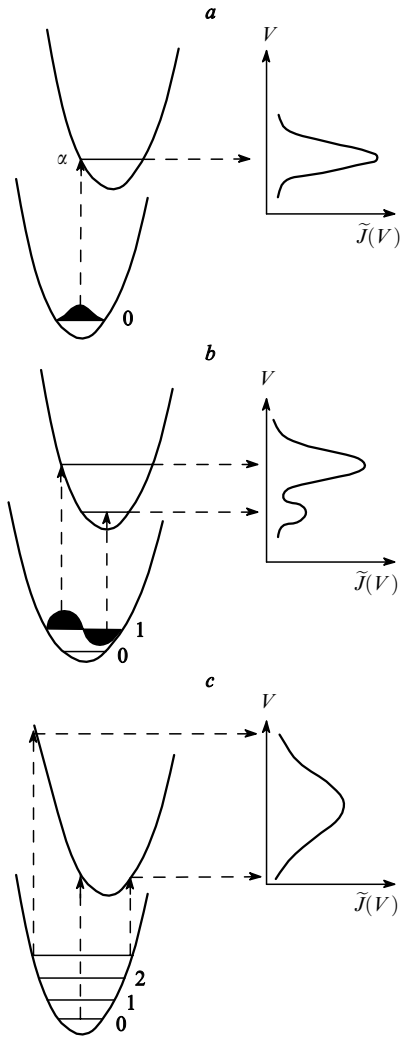


Figure 13. A scheme illustrating the formation of different types of envelopes for the vibrational spectra of adsorbates and the relation between the shape of the envelope and $\tilde{J}(V)$ and distributions over vibrational states.

[‡] It should be mentioned that single molecule spectroscopy by laser induced fluorescence also provides a means for studying the structure of and quantum transitions in single adsorbed species. However, spatially resolved experiments as well as studies on multi-quantum vibrational transitions and those involving highly excited states cannot be performed using this technique. The potentialities of this method have been considered in detail in a special issue of the *Chemical Physics* journal.[66]

[§] It will be recalled that we use the system of atomic units in which the electron charge $e = 1$.

$$n(\upsilon) = \begin{cases} 1, & \upsilon = 0 \\ 0, & \upsilon \neq 0 \,. \end{cases}$$

It will be recalled that usually the condition $kT \ll \omega$ is fulfilled. In this case, all the tunnelling electrons interact with the nonexcited surface complex and the envelopes of the resonance series are determined only by the Franck–Condon factors $\langle 0|\bar{\upsilon}\rangle^2$

$$\langle 0|\bar{\upsilon}\rangle^2 = \frac{\alpha^{\bar{\upsilon}} \exp(-\alpha)}{\bar{\upsilon}!} \,.$$

Here, α is the vibronic coupling parameter equal to the number of the energy level in which the species goes from the ground vibrational state (see Fig. 13 *a*). At $\alpha \approx 1$, the envelopes have a shape of sufficiently narrow bell-shaped curves.¶

For nonequilibrium distributions, the envelopes have a different shape. For Boltzmann-type distributions,

$$n(\upsilon) \approx \exp\left(-\frac{\upsilon}{\langle\upsilon\rangle}\right),$$

the envelopes are also bell-shaped, but have larger halfwidths which depend on $\langle\upsilon\rangle = \sum_{\upsilon} \upsilon n(\upsilon)$ (see Fig. 13 *c*). For inverse distributions, the envelopes exhibit oscillations, *i.e.*, the spectra are formed by groups of resonance maxima on the $J-V$ curves (see Fig. 13 *b*). The number of such groups, N, correlates with the number (υ_m) of the energy level with the highest population

$$N = \upsilon_m + 1.$$

Figures 8–10 present some examples of the vibrational spectra with bell-shaped and oscillating envelopes, obtained in our studies on the initial stages of the oxidation of aluminium at room temperature. The results of calculations of the $J-V$ curves using relationships (17) and (18) show the possibility of reconstructing the nonequilibrium distributions over vibrational states for the surface complexes located under the STM tip and 'heated' by the current of elastically and inelastically tunnelling electrons.

2. Kinetics of multi-quantum vibrational transitions

Combining the solution of equations (17) and calculations of vibrational series of the current–voltage characteristics of the STM using expression (16) allows the kinetics of vibrational transitions in single complexes located under the STM tip to be reconstructed from the experimental $J-V$ curves. Clearly, this also includes the reconstruction of the parameters determining the rate of vibrational relaxation of the surface complex to which the spectrum under study corresponds.

The dependences of the distributions $n(\upsilon)$ and corresponding $J-V$ curves on the excitation and de-excitation rates of vibrational degrees of freedom of surface complexes can be readily illustrated by the results of calculations presented in Figs 14–16. [Full information on the kinetics of vibrational transitions is contained in the shape of the envelopes, therefore the results of calculations of the $J(V)$ dependences are given in relative units.] The histograms of corresponding vibrational distributions calculated using formulae (7), (17) and (18) for both resonance and off-resonance V values are also shown in Figs 14–16.

In accordance with formula (7), the partial tunnelling currents ($J_{\upsilon\upsilon'}$) were approximated by resonance-type terms in which the probabilities of tunnelling from the tip to the trap, Γ_1, and from the trap to the sample, Γ_2, had the form

$$\Gamma_1 = C_1 \exp\left(-\frac{C}{V}\right), \quad \Gamma_2 = \text{const},$$

where C_1 and C are constants.

¶ Mention may be made of an analogy between inelastic resonance tunnelling and resonance absorption of light by molecules [67] and impurity centres in crystals.[68]

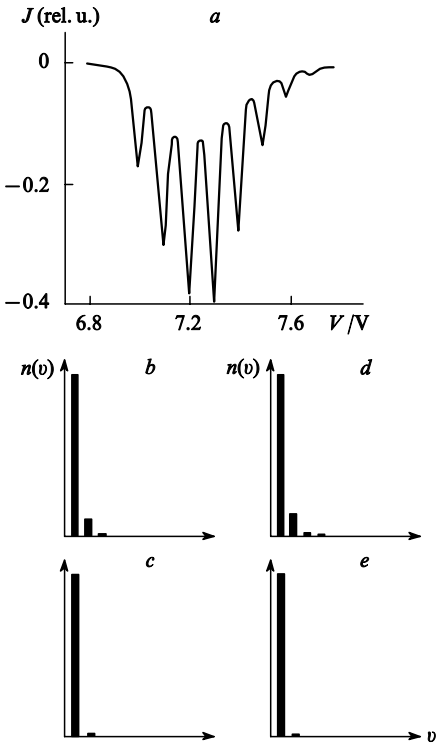


Figure 14. Vibrational spectrum with bell-shaped envelope (*a*) and distributions over vibrational levels (*b*–*e*).
Calculated using formulae (6), (16) and (17) for $w_{r\upsilon} > J_\upsilon$;
V/V: 7 (*b*), 7.05 (*c*), 7.4 (*d*) and 7.45 (*e*).

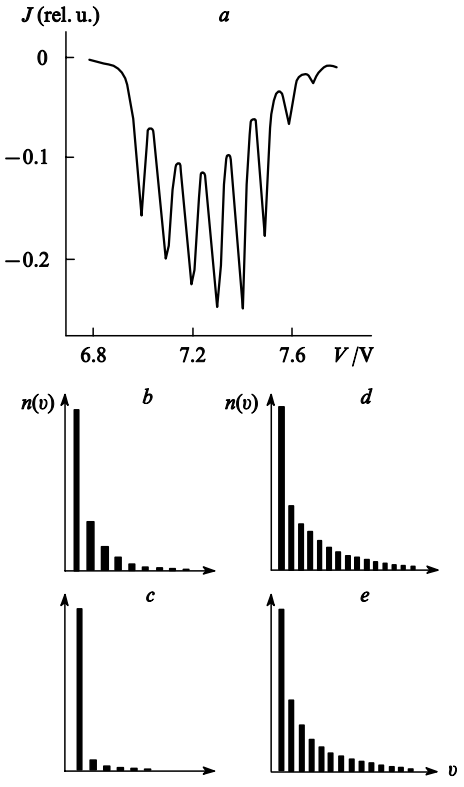


Figure 15. Vibrational spectrum with bell-shaped envelope (*a*) and distributions over vibrational levels (*b*–*e*). Calculated using formulae (6), (16) and (17) for $w_{r\upsilon} < J_\upsilon$; (*b*–*e*) see Fig. 14.

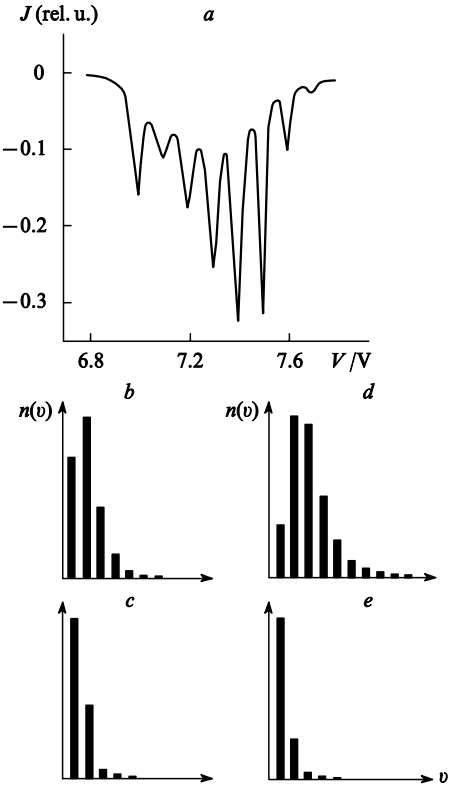


Figure 16. Vibrational spectrum with bell-shaped envelope (*a*) and distributions over vibrational levels (*b*–*e*). Calculated using formulae (6), (16) and (17) for $w_{r\upsilon} < J_\upsilon$, $w_{r\upsilon} \approx \upsilon^3$; (*b*–*e*) see Fig. 14.

Different conditions for the excitation of the vibrational subsystem by the currents $J_{\upsilon\upsilon'}$ and for current-induced and spontaneous (with the rate approximated by the dependence $w_{r\upsilon} = c_r\upsilon^n$) vibrational relaxation were simulated. This was achieved by varying the parameters Γ_1, C_1, C, Γ_2, c_r and n in such a manner that the distributions over vibrational levels corresponded to the histograms presented in Figs 14–16.

The calculated spectrum shown in Fig. 14*a* corresponds to weak heating of the vibrational subsystem (*cf*. Fig. 13*a*). Changes in the bell-shaped spectrum upon an increase in the temperature of the vibrational subsystem are presented in Fig. 15*a* and the relation between the spectra with oscillating envelopes and inverse distributions $n(\upsilon)$ is illustrated by the plot shown in Fig. 16*a*. (This type of distributions is formed if the currents are rather heavy while the vibrational relaxation is slow and its rate is a nonlinear function of the excitation level.)

VII. Scanning tunnelling spectroscopy using fluctuations of STM currents

Pioneering STM studies and direct observation of slow surface migration of species with a time resolution of the order of 0.1 s have been reported more than a decade ago.[69,70] Since then, surface diffusion was repeatedly studied by scanning tunnelling microscopy (see, *e.g.*, Refs 71 and 72). By and large, such experiments are similar to those carried out earlier with a field emission[73] and ion microscope.[74] The known procedure for reconstructing the surface migration parameters from the images taken at different time instants allows one to reconstruct the surface diffusion activation energies of species with a reasonable accuracy (~5%–15%). Unfortunately, the pre-exponential factors in the expressions for the diffusion coefficients are determined with much lower (from 1.5 to 2 orders of magnitude) accuracy. This precludes studies on the surface migration dynamics. In particular, the hop lengths distributions of the migrating species remain unknown so far. These distributions determine the rates of many heterogeneous chemical reactions, but often do not necessarily correspond to the nearest adsorption site.[1]

It is believed that the problem can be solved by studying the spectral characteristics of the noise of tunnelling currents in STM due to changes in the conductance of the tunnelling gap caused by the passage of the migrating species.[28,29,75] An optimum design of experiment using 'fluctuation scanning tunnelling spectroscopy' has been proposed and substantiated.[28,29] Suppose the STM tip scans the surface area containing the migrating species using a velocity close to the migration rate of the species. In this case, the spectral density of the low-frequency noise of the STM current strongly depends not only on the pre-exponential factor in the equation for the diffusion coefficient, but also on time taken for the migrating species to hop from one adsorption site to another one. Since even commercially sold STMs allow the surface scan velocity to be varied over a wide range (from 1 to 100 nm s^{-1}), scanning tunnelling spectroscopy using fluctuations of STM currents can be used for reconstructing the surface migration dynamics of not only slow particles, but also fast ones which cannot be imaged by surface topography measurements.

VIII. Time-resolved scanning tunnelling spectroscopy

Rapid progress in femtosecond laser spectroscopy and scanning tunnelling spectroscopy allows the surface structure to be studied with atomic-scale spatial or corresponding time resolution. This makes it possible to pose a more complicated problem of integrating the capabilities of these modern, powerful experimental methods for studying the surface.

Pioneering studies aimed at integrating the probe methods of studying solid surfaces including scanning tunnelling microscopy and femtosecond laser spectroscopy date back to early 1990s.[76–79] Currently, two main research avenues have been developed, the optical and tunnelling one, each with its specific problems and solution methods. To review them goes beyond the scope of this paper, so we will only briefly outline the state-of-the-art in the field.

In optical studies, the STM tip is replaced by a thin optical fibre brought to the surface under study to a distance shorter than the light wavelength. This type of probe instruments, *viz*., near-field scanning optical microscopes, provides atomic-scale time resolution in combination with rather high spatial resolution (~30–50 nm), which is one or two orders of magnitude higher than the resolution of conventional optical microscopes.

To achieve higher spatial resolution, one needs continue in use experimental methods employing STMs. Using the STM also allows time-resolved spectroscopic measurements to be performed by varying the conductance of the tunnel junction. As follows from expression (2), this can be done by varying the tunnelling gap or by changing the surface density of electron states (*e.g.*, by illuminating the contact) or the voltage. Each of these approaches has its own limitations that are due to inertia of the tip, finite switching rate of control circuits and small magnitudes of the tunnelling currents. Currently, time resolution achieved in experiments with STMs is no better than several picoseconds,[80] though integration of STM and femtosecond laser spectroscopy has been the subject of research activity in many research centres.

IX. Conclusion

The history of development of scanning tunnelling microscopy and spectroscopy demonstrates numerous examples of successful solutions to fundamental problems of surface chemistry and physics. One cannot but be surprised at increasing number of new possibilities provided by the STM, the perfect scientific instrument. Advanced research techniques in surface chemistry and physics owe their origin to the creators of the STM. On the other hand, mention should be made of rapid increase in applied

research in which the STM and related probe instruments (see a short review [80]) are used as instruments for assembling of various nanoclusters from individual atoms on the solid surfaces. Nanoclusters exhibit unique physical and chemical properties. For instance, they can be extremely hard and possess high adsorptive and emissive capacities and reactivity. The conductivity of nanoclusters can be controlled in a targeted manner by varying their atomic structure without changing the chemical composition, by doping them with individual impurity atoms or by applying mechanical strain or a magnetic field. Of course, this gives rise to lots of ideas associated with possible use of both single 'hand-assembled' nanoclusters and multicluster nanomaterials in different areas of chemistry, in electronics, technology, ecology, medicine, *etc*. The development of nanotechnologies also implies wide use of probe instruments. Crucial importance of nanotechnologies to high-tech processes of the 21st century has now gained general acceptance in all highly developed countries. It is a wide-spread, well-substantiated opinion that many economic, military, social, political and medicinal problems can be solved using the results of nanotechnological studies. There are strong grounds to believe that the mission of being a scientific basis for nanotechnologies falls to the single molecule chemical physics of surfaces, which has been rapidly developed in a manner much like that of the chemical physics of macroscopic ensembles of atomic species.

The authors express their gratitude to Academician A L Buchachenko for incessant support of their research, frequent discussions of the results obtained, valuable comments and criticism. We are also grateful to M V Sharova for help in preparing the manuscript.

This review has been written with the financial support of the Russian Foundation for Basic Research (Project Nos 99-03-32098 and 99-03-32100).

References

1. O V Krylov, B R Shub *Neravnovesnye Protsessy v Katalize* (Non-Equilibrium Processes in Catalysis) (Moscow: Khimiya, 1990)
2. O V Krylov, V F Kiselev *Adsorbtsiya i Kataliz na Perekhodnykh Metallakh i Ikh Oksidakh* (Adsorption and Catalysis on Transition Metals and Their Oxides) (Moscow: Khimiya, 1981)
3. L A Bol'shov, A P Napartovich, A G Naumovets, A G Fedorus *Usp. Fiz. Nauk* **122** 125 (1978) [a]
4. *Handbook of Microscopy. Application in Materials Science. Solid State Physics and Chemistry* (Weinheim: VCH, 1997)
5. M W Roberts, C S McKee *Chemistry of the Metal–Gas Interface* (Oxford: Oxford University Press, 1979)
6. H L Dai, W Ho (Eds) *Laser Spectroscopy and Photochemistry on Metal Surfaces* (Singapore: World Sci., 1995)
7. G Binnig, H Rohrer, Ch Gerber, E Weibel *Phys. Rev. Lett.* **49** 57 (1982)
8. R Wiensendanger *Scanning Probe Microscopy and Spectroscopy*. (Cambridge: Cambridge University Press, 1994)
9. J Tersoff, D R Hamann *Phys. Rev. B* **31** 805 (1985)
10. H-J Gunterrodt, R Wiesendanger (Eds) *Scanning Tunnelling Microscopy III. Springer Series in Surface Science* (Berlin: Springer, 1993)
11. R Z Bakhtizin, T Hashizume, X-D Wang, T Sakurai *Usp. Fiz. Nauk* **167** 289 (1997) [a]
12. D M Eigler, E K Schweizer *Nature (London)* **344** 524 (1991)
13. B C Stipe, M A Rezaei, W Ho, S Gaom, M Persson, B I Lindqvist *Phys. Rev. Lett.* **78** 4410 (1997)
14. L J Lauhon, W Ho *Phys. Rev. Lett.* **84** 1527 (2000)
15. Ph Avouris *Acc. Chem. Res.* **28** (3) 95 (1995)
16. A L Buchachenko *Usp. Khim.* **68** 99 (1999) [*Russ. Chem. Rev.* **68** 85 (1999)]
17. B C Stipe, M A Rezaei, W Ho *Science* **280** 1732 (1998)
18. F I Dalidchik, M V Grishin, S A Kovalevskii, N N Kolchenko *Pis'ma Zh. Eksp. Teor. Fiz.* **65** 306 (1997)
19. M V Grishin, F I Dalidchik, S A Kovalevskii, N N Kolchenko *Pis'ma Zh. Eksp. Teor. Fiz.* **71** 104 (2000)
20. F I Dalidchik, M V Grishin, S A Kovalevskii, N N Kolchenko, B R Shub *Poverkhnost'* **6** 107 (2001)
21. M V Grishin, F I Dalidchik, S A Kovalevskii, N N Kolchenko, B R Shub, in *Zondovaya Mikroskopiya-2001 (Materialy Vserossiiskogo Soveshchaniya), Nizhnii Novgorod, 2001* [Probe Microscopy-2001 (Proceedings of All-Russian Meeting), Nizhnii Novgorod, 2001] p. 131
22. E M Balashov, S O Gladkov, F I Dalidchik, M A Kozhushner, B R Shub *Khim. Fiz.* **20** (5) 85 (2001) [b]
23. E Balashov, S Gladkov, F Dalidchik, M Kozhushner, B Shub *Phys. Lett. A* **282** 47 (2001)
24. F I Dalidchik, S A Kovalevskii *Pis'ma Zh. Eksp. Teor. Fiz.* **67** 916 (1998)
25. A L Buchachenko, M A Kozhushner, B R Shub *Izv. Akad. Nauk, Ser. Khim.* 1732 (1998) [c]
26. M A Kozhushner, B R Shub, R R Muryasov *Pis'ma Zh. Eksp. Teor. Fiz.* **67** 484 (1998)
27. A L Buchachenko, F I Dalidchik, S A Kovalevskii, B R Shub *Usp. Khim.* **70** 613 (2001) [*Russ. Chem. Rev.* **70** (7) (2001)]
28. A S Prostnev, V I Chernysh, B R Shub *Khim. Fiz.* **16** (6) 25 (1997) [b]
29. A Prostnev,V Chernysh, B Shub *Chem. Phys. Rep.* **18** 13 (1997)
30. D Bohm *Quantum Mechanics* (New York: Prentise Hall Inc., 1952)
31. F I Dalidchik *Zh. Eksp. Teor. Fiz.* **87** 1384 (1984)
32. F Dalidchik, M Grishin, N Kolchenco, S Kovalevskii, in *Book of Abstracts of the 43rd International Field Emission Symposium, Moscow, 1996* p. 25
33. F Dalidchik, M Grishin, N Kolchenco, S Kovalevskii *Surf. Sci.* **387** 50 (1997)
34. G Binnig, K H Frank, H Fuchs, N Garsia, B Rehl, H Rohrer, F Salvan, A R Williams *Phys. Rev. Lett.* **55** 991 (1985)
35. R S Becker, J A Golovchenko, B S Swartzentruber *Phys. Rev. Lett.* **55** 987 (1985)
36. I-W Lyo, Ph Avouris *Science* **245** 1369 (1989)
37. N D Lang *Phys. Rev. B* **55** 9364 (1997)
38. F Dalidchik, M Grishin, N Kolchenko, S Kovalevskii, B Shub *Spectrosc. Lett.* **30** 1429 (1997)
39. F Dalidchik, M Grishin, N Kolchenko, S Kovalevskii *Ultramicroscopy* **79** 203 (1999)
40. F I Dalidchik, M V Grishin, S A Kovalevskii, N N Kolchenko, B R Shub *Pis'ma Zh. Eksp. Teor. Fiz.* **66** 37 (1997)
41. S A Kovalevskii, F I Dalidchick, M V Grishin, N N Kolchenko, B R Shub *Appl. Phys. A, Mater. Sci. Process.* **66** (Suppl. Pt.1) (1988)
42. S A Kovalevskii, F I Dalidchick, M V Grishin, B R Shub, in *Preliminary Proceedings of STM'99, Seoul, Korea, 1999* p. 673
43. M Grishin, F Dalidchik, S Kovalevskii, N Kolchenko, in *Book of Abstracts of the 45th International Field Emission Symposium, Irbid, Jordan, 1998* p. 74
44. R C Jaklevic, J Lambe *Phys. Rev. Lett.* **17** 1139 (1966)
45. V I Fistul', N Z Shvarts *Usp. Fiz. Nauk* **77** 109 (1962) [a]
46. N Holonyak, I F Lesk *Phys. Rev. Lett.* **4** 3167 (1959)
47. P K Hansma *Tunnelling Spectroscopy: Capabilities, Applications and New Techniques* (New York: Plenum, 1982)
48. B N J Persson, J E Dimuth *Solid State Commun.* **57** 769 (1986)
49. B N J Persson, A Baratoff *Phys. Rev. Lett.* **59** 339 (1987)
50. B C Stipe, M A Rezaei, W Ho *Rev. Sci. Instrum.* **70** 137 (1999)
51. J K Gimzevski, Ch Joachim *Science* **283** 1683 (1999)
52. J Gaudioso, H J Lee, W Ho *J. Am. Chem. Soc.* **121** 8479 (1999)
53. L J Lauhon, W Ho *Phys. Rev. B* **60** R8525 (1999)
54. C J Noble, P G Burke *Phys. Rev. Lett.* **68** 2011 (1992)
55. A A Davydov *IK Spektroskopiya v Khimii Poverkhnosti Okislov* (IR Spectroscopy in the Chemistry of Oxides Surface) (Novosibirsk: Nauka, 1984)
56. H Ibach, in *Electron Energy Loss Spectrometers. Springer Series in Optical Sciences* (Berlin: Springer, 1990)
57. M B Hugenschmidt, L Gamble, C T Campbell *Surf. Sci.* **302** 329 (1994)
58. I V Zakurdaev, D S Firsov, in *Zondovaya Mikroskopiya-99 (Materialy Vserossiiskogo Soveshchaniya), Nizhnii Novgorod, 1999* [Probe Microscopy-99 (Proceedings of All-Russian Meeting), Nizhnii Novgorod, 1999] p. 283
59. H Brune, J Witterlin, J Trost, G Ertl, J Wiechers, R J Behm *J. Chem. Phys.* **99** 2128 (1993)
60. C Astaldi, P Geng, K Jakoby *J. Electron. Spectrosc. Relat. Phenom.* **44** 175 (1987)
61. J L Erskine, R L Strong *Phys. Rev. B* **25** 5547 (1982)
62. A B Roitsin, V M Maevskii *Usp. Fiz. Nauk* **159** 297 (1989) [a]

63. Y Manassen, R J Hamers, J E Demuth, A J Castellano Jr *Phys. Rev. Lett.* **62** 2531 (1989)
64. D Shadal, Y Manassen *Phys. Rev. B* **44** 11528 (1991)
65. M V Grishin, F I Dalidchik, S A Kovalevskii, N N Kolchenko, B R Shub, in *Zondovaya Mikroskopiya-99 (Materialy Vserossiiskogo Soveshchaniya), Nizhnii Novgorod, 1999* [Probe Microscopy-99 (Proceedings of All-Russian Meeting), Nizhnii Novgorod, 1999] p. 63
66. *Chem. Phys.* **247** (1) (Spec. Issue) (1999)
67. M D Frank-Kamenetskii, A V Lukashin *Usp. Fiz. Nauk* **116** 193 (1975) [a]
68. G Ehrlich, F Hudda *J. Chem. Phys.* **35** 1421 (1961)
69. Y-W Mo, B S Swartrantruber, M B Webb, M L Lagally *J. Vac. Sci. Technol. A* **8** 201 (1990)
70. E Ganz, K Sattler, J Clarke *Surf. Sci.* **219** 33 (1989)
71. E Ganz, S Theiss, I-S Hwang, J Golovchenko *Phys. Rev. Lett.* **68** 1567 (1992)
72. Y-W Mo *Phys. Rev. Lett.* **71** 2923 (1993)
73. R Gomer *Rep. Progr. Phys.* **53** 917 (1990)
74. E W Müller, T T Tsong *Field Ion Microscopy. Field Ionization and Evaporation)* (Oxford: Pergamon Press; Translated into Russian; Moscow: Nauka, 1980)
75. M Sumetskii, A Kornyshev *Phys. Rev. B* **48** 17493 (1993)
76. M R Freeman, G Nunes Jr *Appl. Phys. Lett.* **63** 2633 (1993)
77. S Weiss, D F Ogletree, D Botkin, M Salmeron, D S Chemla *Appl. Phys. Lett.* **63** 2567 (1993)
78. J W P Hsu, E A Fitzgerald, Y H Xie, P J Silverman *J. Appl. Phys.* **79** 7743 (1996)
79. M J Gregor, P G Blome, R G Ulbrich, Grossmann, S Grosse, J Feldmann, W Stolz, E O Göbel, D J Arent, M Bode, K A Bertness, J M Olson *Appl. Phys. Lett.* **67** 3572 (1995)
80. R Pool *Science* **247** 634 (1990)

[a] — *Physics-Uspekhi (Engl. Transl.)*
[b] — *Chem. Phys. Rep. (Engl. Transl.)*
[c] — *Russ. Chem. Bull. (Engl. Transl.)*